

Supporting information

High-temperature-triggered crosslinking reaction to achieve excellent intrinsic flame retardancy of organic phase change composite

Jingkai Liu ^a, Yunyun Xiao ^c, Yiqing Wang ^a, Yishun Wuliu ^a, Xinbei Zhu ^{a, b},
Liyue Zhang ^a, Xiaoqing Liu ^{a*}

^a Key Laboratory of Advanced Marine Materials, Ningbo Institute of Materials
Technology and Engineering (NIMTE) of the Chinese Academy of Sciences (CAS),
Ningbo 315201, P. R. China

^b University of Chinese Academy of Sciences, Beijing 100049, P. R. China

^c International Institute for Innovation, Jiangxi University of Science and
Technology, Nanchang 330013, P.R. China

*Author for the Correspondence: liuxq@nimte.ac.cn

This PDF file includes:

1. Experimental section
2. Figure S1-S40
3. Equation S1-S5
4. Table S1-S4
5. References 1-18

1. Experimental section

1.1 materials

Pyrogallol (AR), 1,3-diaminopropane (AR), 1,6-diaminohexane (AR), aniline (AR), and paraformaldehyde (AR) were purchased from Aladdin Reagent Co., Inc. 3-pentadecylphenol (AR) and 1,12-diaminododecane (AR) were all purchased from Energy Chemical. Co., Ltd. Sodium hydroxide (AR), Magnesium sulfate (AR), Ethanol (AR), Toluene (AR), N,N-Dimethylformamide (AR), Hydrochloric acid (AR), Ethyl acetate (AR) and Acetone (AR) were obtained from Sinopharm Chemical Reagent Co., Ltd. All chemicals were used without further purification.

1.2 Synthesis of benzoxazine-based PCMs

In a typical experiment, 1,3-diaminopropane (2.22 g, 0.03 mol), 3-pentadecylphenol (18.27 g, 0.06 mol), and paraformaldehyde (3.60 g, 0.12 mol) were mixed in 100 ml round bottom flask. 50 ml toluene was added as a solvent, and the reaction system was stirred and refluxed for 6 h at 105 °C. After the reaction, it was cooled to room temperature and filtered to remove the insoluble matter. The filtrate was collected and washed three times with 1 mol/L sodium hydroxide solution and deionized water respectively. The organic phase was dried with anhydrous sodium sulfate. Finally, the crude yellow product was obtained by vacuum distillation to remove the solvent, and the precipitate was recrystallized from ethanol as a white powder (yield 86.8%). C-dah and C-dap were prepared by using 1,6-diaminohexane or 1,12-diaminododecane as raw materials with similar procedures (yield 85.3% and 88.1%).

1.3 Synthesis of aerogel precursor (PY-a)

The synthetic route of PY-a is shown in scheme 1. Aniline (9.32 g, 0.10 mol) and paraformaldehyde (7.51 g, 0.25 mol) were added to a three-necked flask with mechanical stirring and condenser, and the temperature was slowly raised to 70 °C and stirred for 3 hrs. Then Pyrogallol (6.31 g, 0.05 mol) was added and refluxed at 70 °C for 3 hrs. After the reaction was completed, it was cooled to room temperature, and the crude product was filtered and washed with ice ethanol. Finally, the white crystal was

obtained by drying (yield 89.4%).

1.4 Preparation of polybenzoxazine aerogels

Polybenzoxazine aerogels (PB-n) were prepared by sol-gel and freeze-drying methods. The PY-a monomer was added to DMF solvent and stirred for 15 min until the monomer was completely dissolved. Then 8 mol/L HCl was added and stirred for 20 min, and the obtained sol was poured into the prepared mold and gelled at room temperature. To intensively study the structure and performance of PB-n aerogels, the monomer concentrations varied from 2.8, 3.9, 4.8, and 7.1 wt.% were set. The gelation time of all samples was 24 h and aged at room temperature for 48 h. Subsequently, all wet gels were removed from the mold and washed with DMF (3x, 12 hrs each time), ethanol (3x, 12 hrs each time), and water (3x, 12 hrs each time). Finally, the PB-n aerogels were obtained by freeze-drying. For simplicity, PB-1, PB-2, PB-3, and PB-4 were used to represent samples with monomer concentrations of 2.8, 3.9, 4.8, and 7.1 wt.%, respectively.

1.5 Preparation of phase change composite

Phase change aerogel composite was prepared by vacuum impregnation. The PCMs (C-dad) were added to a 25 ml beaker in a vacuum oven and heated up to 100 °C for complete melting. Then put the aerogel into the beaker, and keep the vacuum degree at 0.1 MPa. Remove the aerogel after there were no bubbles, and the residual PCMs on the surface were wiped off. After cooling to room temperature, the aerogel phase change composite material was obtained, namely PB-1/C-dad, PB-2/C-dad, PB-3/C-dad, and PB-4/C-dad, respectively.

1.6 Combustion experiment

An appropriate amount (~50 mg) of the sample was first placed in a 6.8 * 4.0 mm (diameter * height) alumina crucible, with a stainless-steel pad at the bottom. Subsequently, a flame generated by a 1600W flame gun (with a maximum temperature of 1500 °C) was used to ignite the sample, of which the outer flame was used to ensure

a similar combustion temperature. During ignition, the combustion behavior was recorded by picture recording. After burning for ~60 s, the fire was removed, and the char residues were collected for further analysis.

1.7 Gel content

The gel content of the samples was determined from the change of its weight as a result of Soxhlet extraction. First, C-dad and PB-1/C-dad were heated at 270 °C for 2 hours to ensure that the crosslinking reaction was completed. After that, about 1 gram of cured samples were packed into a filter paper and added into the Soxhlet extractor for the extraction of soluble components with acetone (200 mL) for 24 h at 60 °C. Finally, dry the insoluble components in an oven for 6 hours, and then weigh them. The gel content can be obtained by dividing these results by the related original mass.

1.8 Chemical structure information of the synthesized benzoxazine monomer

1,3-bis(7-pentadecyl-2*H*-benzo[*e*][1,3]oxazin-3(4*H*)-yl)propane (C-dap): ¹H NMR (600 MHz, CDCl₃, 25 °C) δ = 6.84, 6.68, 6.60, 4.83, 3.94, 2.74, 2.72, 2.70, 2.53, 2.51, 2.49, 1.59, 1.57, 1.56, 1.54, 1.36, 1.35, 1.34, 1.33, 1.32, 1.30, 1.29, 1.25, 0.90, 0.88, 0.87, 0.86. ¹³C NMR (151 MHz, CDCl₃) δ = 153.93, 142.89, 127.28, 120.79, 117.23, 116.09, 82.46, 50.12, 49.05, 35.69, 31.93, 31.37, 29.70, 29.69, 29.59, 29.53, 29.37, 29.34, 26.76, 22.70, 14.13. FT-IR (cm⁻¹): 3436, 2955, 2917, 2849, 1621, 1574, 1506, 1470, 1333, 1242, 1162, 1134, 983, 890, 797, 718. Elem. Anal. Calc. for C₄₉H₈₂N₂O₂: C, 80.49; H, 11.30; N, 3.83; O, 4.38. m/z [M⁺H]⁺ (amu): 730.21 (calculated), 731.21 (observed).

1,6-bis(7-pentadecyl-2*H*-benzo[*e*][1,3]oxazin-3(4*H*)-yl)hexane (C-dha): ¹H NMR (600 MHz, CDCl₃, 25 °C) δ = 7.26, 6.86, 6.84, 6.70, 6.68, 6.60, 4.83, 3.94, 2.74, 2.72, 2.70, 2.53, 2.51, 2.50, 1.63, 1.61, 1.59, 1.57, 1.56, 1.54, 1.37, 1.36, 1.35, 1.34, 1.33, 1.32, 1.30, 1.29, 1.29, 1.25, 0.90, 0.88, 0.87, 0.86. ¹³C NMR (151 MHz, CDCl₃) δ = 153.95, 142.85, 127.27, 120.76, 117.30, 116.06, 82.40, 51.26, 50.08, 35.69, 31.93, 31.37, 29.71, 29.69, 29.59, 29.53, 29.37, 29.35, 28.06, 27.11, 22.70, 14.13. FT-IR (cm⁻¹): 3454, 2954, 2919, 2850, 1620, 1576, 1505, 1468, 1429, 1330, 1242, 1158, 1144,

1117, 1020, 982, 962, 869, 791, 721. Elem. Anal. Calc. for C₅₂H₈₈N₂O₂: : C, 80.77; H, 11.47; N, 3.62; O, 4.14. m/z [M⁺H]⁺ (amu): 771.68 (calculated), 772.68 (observed).

1,12-bis(7-pentadecyl-2*H*-benzo[*e*][1,3]oxazin-3(4*H*)-yl)dodecane (C-dda): ¹H NMR (600 MHz, CDCl₃, 25 °C) δ = 7.26, 6.86, 6.84, 6.70, 6.70, 6.68, 6.68, 6.60, 6.60, 4.84, 3.96, 2.74, 2.72, 2.71, 2.54, 2.52, 2.50, 1.60, 1.58, 1.57, 1.56, 1.55, 1.54, 1.53, 1.33, 1.32, 1.31, 1.30, 1.29, 1.28, 1.26, 0.90, 0.88, 0.86. ¹³C NMR (151 MHz, CDCl₃) δ = 154.00, 142.83, 127.29, 120.73, 117.39, 116.06, 82.43, 51.41, 50.12, 35.71, 31.95, 31.39, 29.72, 29.70, 29.67, 29.61, 29.60, 29.55, 29.39, 29.36, 28.19, 27.27, 22.71, 14.15. FT-IR (cm⁻¹): 3443, 2957, 2917, 2849, 1621, 1576, 1506, 1470, 1435, 1242, 1137, 1124, 987, 971, 885, 870, 797, 718. Elem. Anal. Calc. for C₅₈H₁₀₀N₂O₂: C, 81.25; H, 11.76; N, 3.27; O, 3.73. m/z [M⁺H]⁺ (amu): 856.45 (calculated), 857.45 (observed).

3,7-diphenyl-3,4,7,8-tetrahydro-2*H*,6*H*-benzo[1,2-*e*:5,4-*e'*]bis([1,3]oxazine)-10-ol (PY-a): ¹H NMR (600 MHz, DMSO, 25 °C) δ = 8.37, 7.28, 7.28, 7.26, 7.24, 7.15, 7.13, 6.91, 6.89, 6.87, 6.37, 5.43, 4.57. ¹³C NMR (151 MHz, DMSO) δ = 148.41, 141.97, 133.28, 129.53, 120.91, 117.98, 114.20, 114.05, 79.29, 48.83. FT-IR (cm⁻¹): 3241, 3002, 2901, 2852, 1598, 1497, 1470, 1359, 1336, 1308, 1270, 1248, 1215, 1183, 1167, 1085, 1069, 978, 939, 829, 786, 769, 753, 706. Elem. Anal. Calc. for C₂₂H₂₀N₂O₃: C, 73.32; H, 5.59; N, 7.77; O, 13.32. m/z [M⁺H]⁺ (amu): 360.15 (calculated), 361.15(observed).

1.9 Characterizations

¹H and ¹³C nuclear magnetic resonance (NMR) spectra of all benzoxazine monomers were recorded on 600 MHz AVANCE NEO 600 (Bruker, Switzerland) in which CDCl₃ and DMSO were used as solvents and tetramethyl silane as an internal standard reagent. The chemical structures of all samples were analyzed by NICOLET 6700 (Thermo, America) Fourier transform infrared spectroscopy (FT-IR) by KBr method with the scanning range of 400-4000 cm⁻¹, and each specimen was scanned 32 times. The elemental analysis was carried out on the Elementar system (Elementar, Germany) and each sample was tested three times to obtain the average value. High-resolution mass spectra (HRMS) were measured by LC-Q-TOF (AB Sciex, America) using ionization

and 500 V ionization voltages at 500 °C. Differential scanning calorimetry (DSC) measurement was carried out on a TGA/DSC I (Mettler Toledo, Switzerland) with a nitrogen flow of 50 ml/min, and the heating rate was 10 °C/min. All samples were analyzed within the appropriate temperature range. Thermogravimetric analysis (TGA) was analyzed on TGA/DSC I (Mettler Toledo, Switzerland). Each specimen was heated from 50 to 800 °C (the heating rate was 20 °C/min), and the purge gas was high-purity nitrogen (the flow rate is 50 mL/min). The surface area was determined by the Brunauer-Emmett-Teller (BET) method based on an ASAP 2460 (Micromeritics, America), and the pore size distribution in desorption branches was calculated by Barrett-Joyner-Halenda (BJH). Thermal conductivity was determined by an LFA457 laser thermal conduction analyzer (NETZSCH, Germany), in which the sample size was 10 mm * 10 mm * 2 mm. X-ray diffraction (XRD) was performed on a Bruker D8 ADVANCE automatic diffractometer with Cu-K α radiation, and the scan rate was 6°/min from 5 to 90°. Polarized optical microscopy (POM) was conducted at GX71 (OLYMPUS, Japan) equipped with a heating stage. Microscale combustion calorimetry (MCC) was performed on an MCC-3 (DEATAK, America), and the sample (~ 5 mg) was heated from 100 to 700 °C with 1 °C/min in a nitrogen atmosphere. The scanning electron microscope (SEM) and energy dispersive spectroscopy (EDS) were obtained on an EVO18 scanning electron microscope (ZEISS, Germany). After the samples were coated with a thin platinum layer, the images were obtained on Thermo Scientific Verios G4 UC. X-ray photoelectron spectra (XPS) were obtained on a Kratos Axis Ultra DLD (Kratos, Japan) and the excitation source was. The atomic composition of the carbon layer surface of the composite PCMs after combustion was analyzed by XPS, using a Kratos Axis Ultra DLD (Kratos, Japan) with the Mg K α excitation source.

2. Figure S1-S40

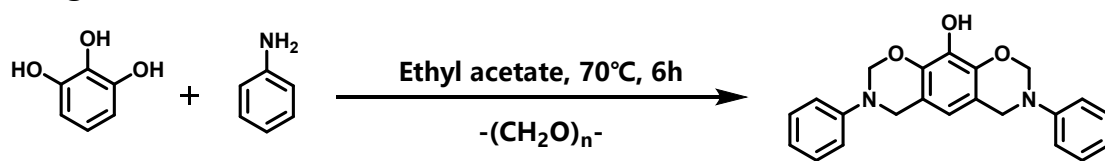


Fig. S1 Synthesis route of PY-a

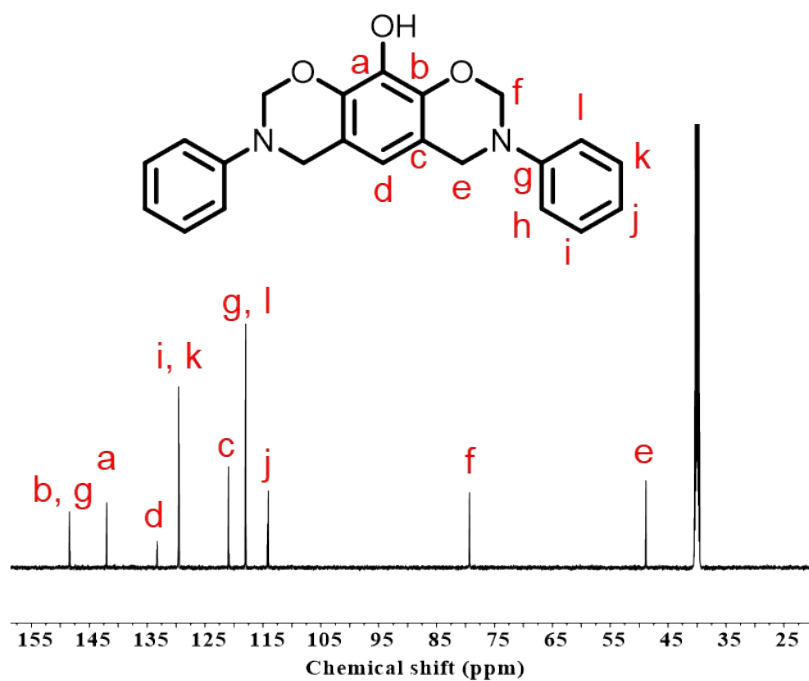


Fig. S2 ^{13}C NMR spectrum of PY-a

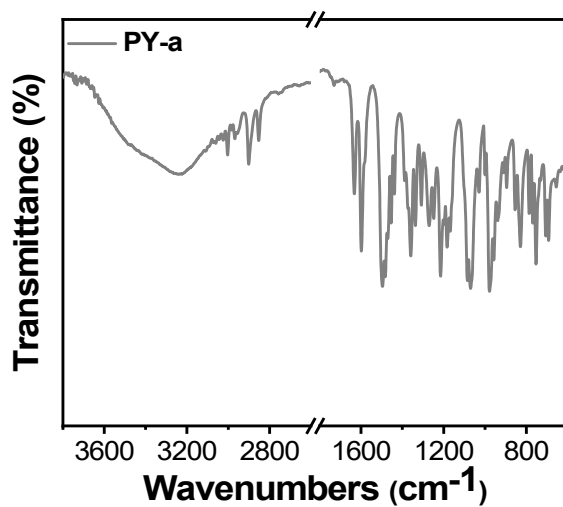


Fig. S3 FT-IR spectrum of PY-a

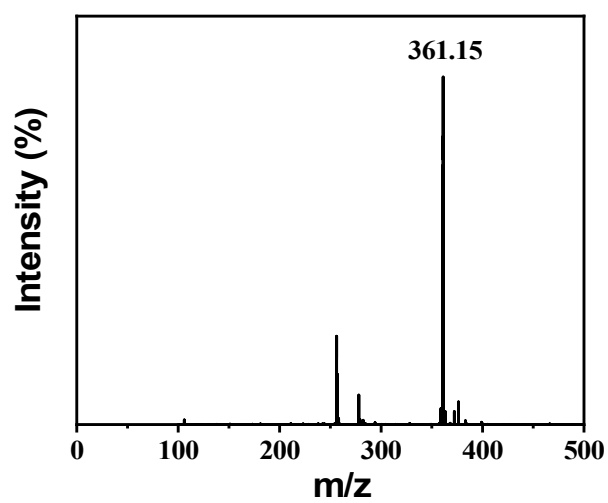


Fig. S4 HRMS of PY-a

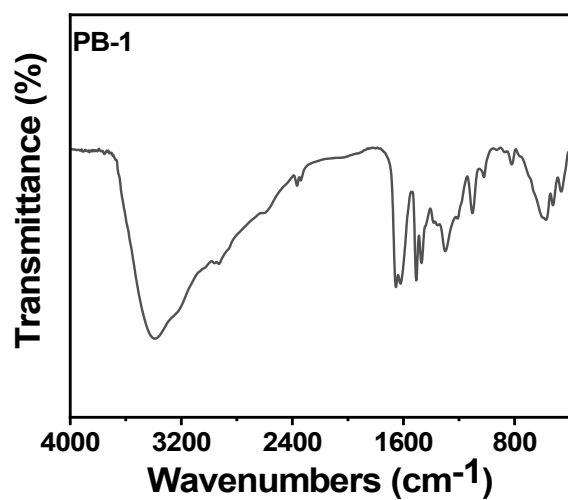


Fig. S5 FT-IR of poly(PY-a) aerogel

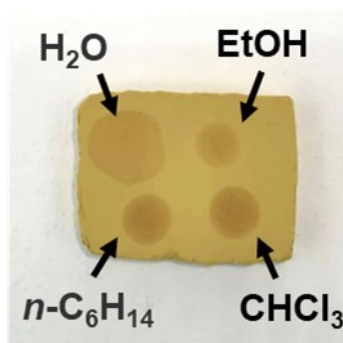


Fig. S6 Solvent wettability of poly(PY-a) aerogel

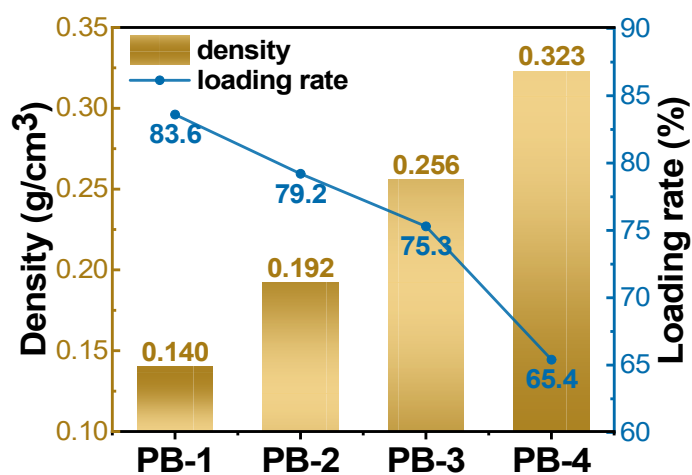


Fig. S7 Density and loading rate of different poly(PY-a) aerogels

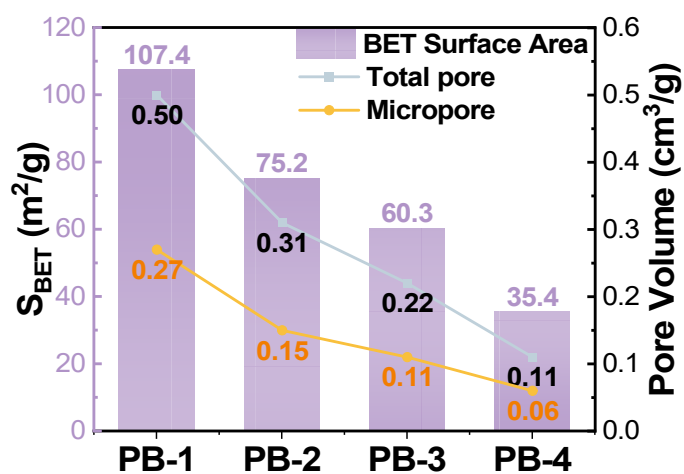


Fig. S8 BET surface area and pore volume of different poly(PY-a) aerogels

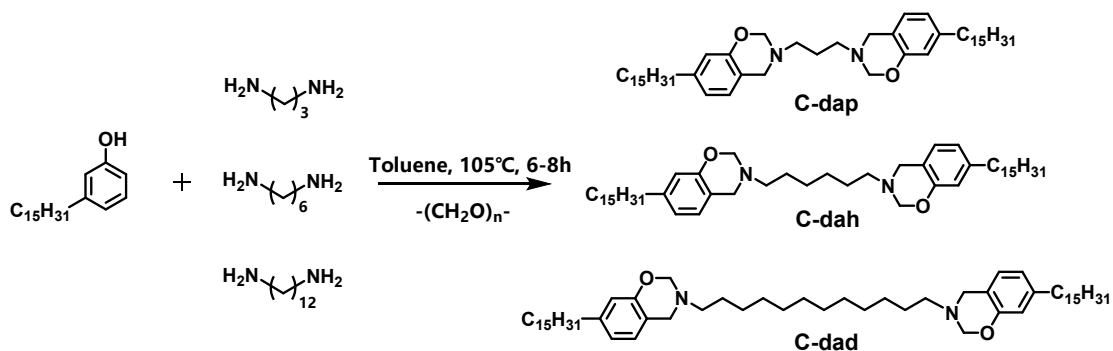


Fig. S9 Synthesis route of the benzoxazine-based PCMs

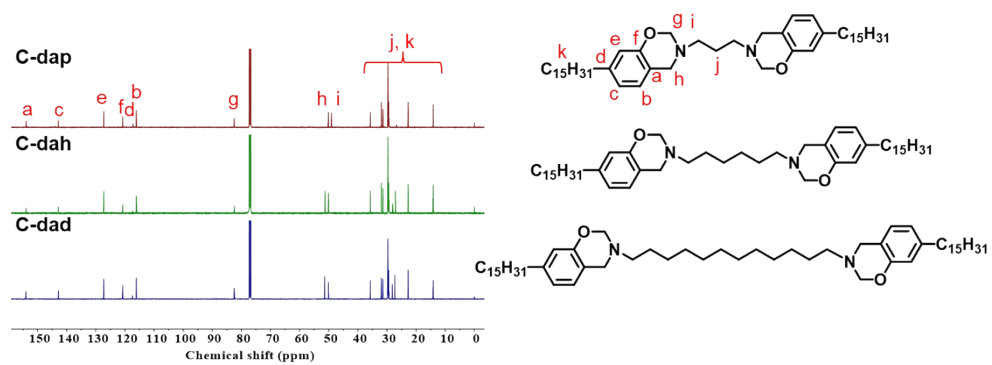


Fig. S10 ^{13}C NMR spectrum of different benzoxazine monomers

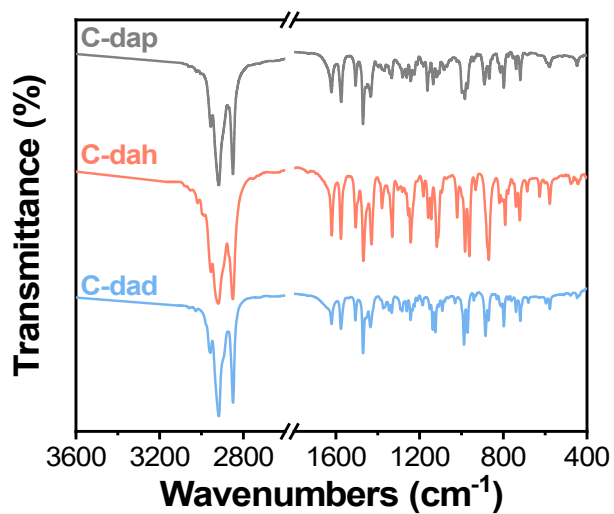


Fig. S11 FT-IR of three benzoxazine monomers

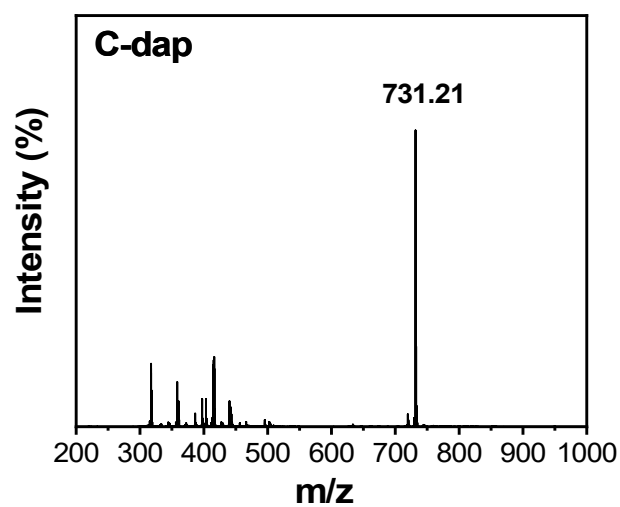


Fig. S12 HRMS of C-dap

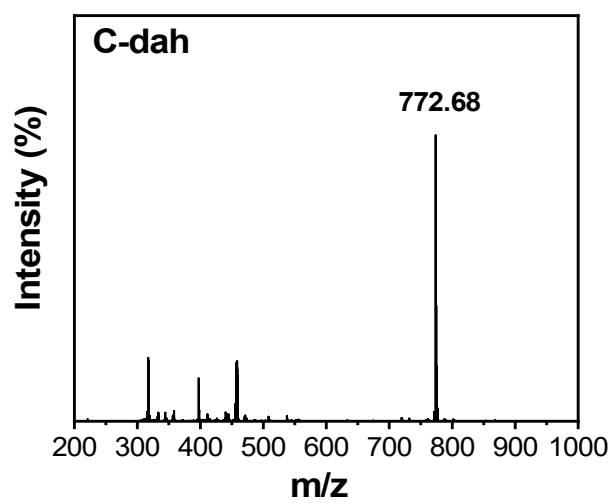


Fig. S13 HRMS of C-dah

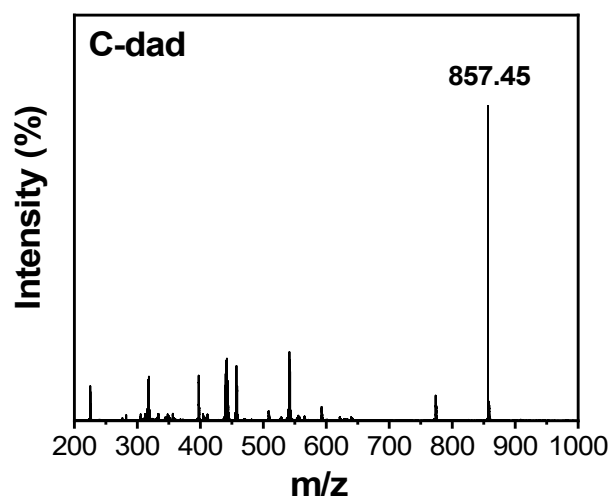


Fig. S14 HRMS of C-dad

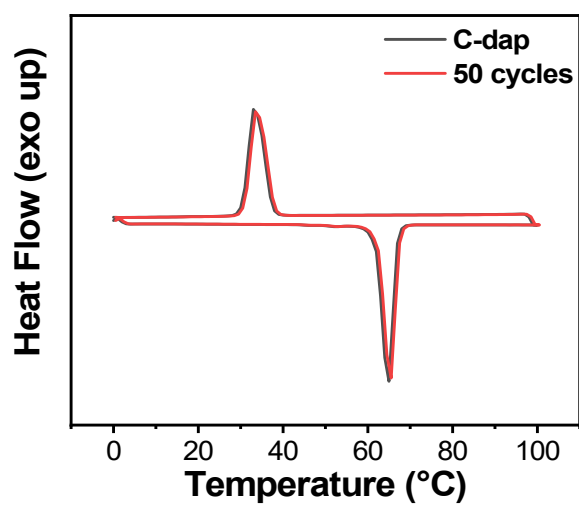


Fig. S15 Cycles stability of C-dap

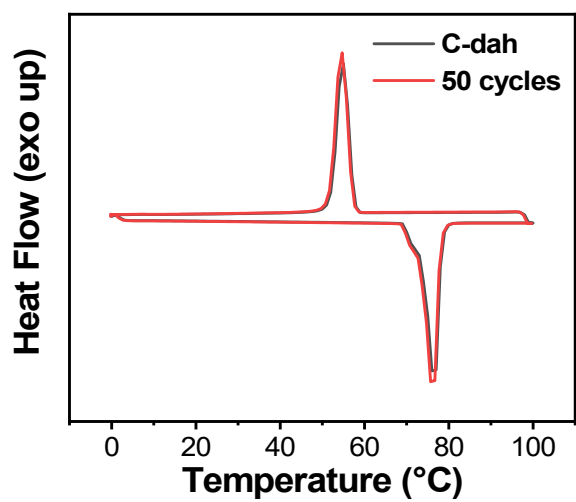


Fig. S16 Cycles stability of C-dah

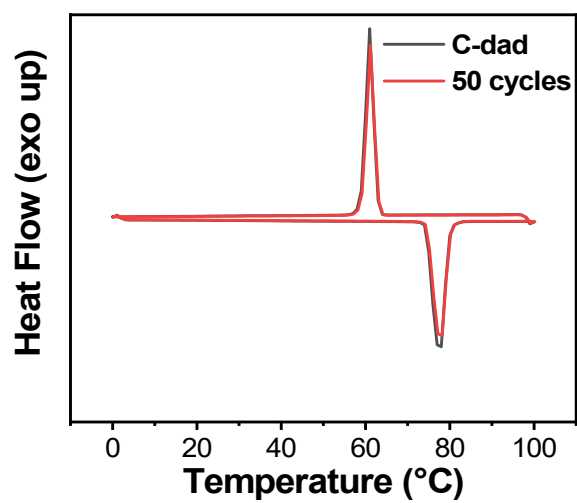


Fig. S17 Cycles stability of C-dad

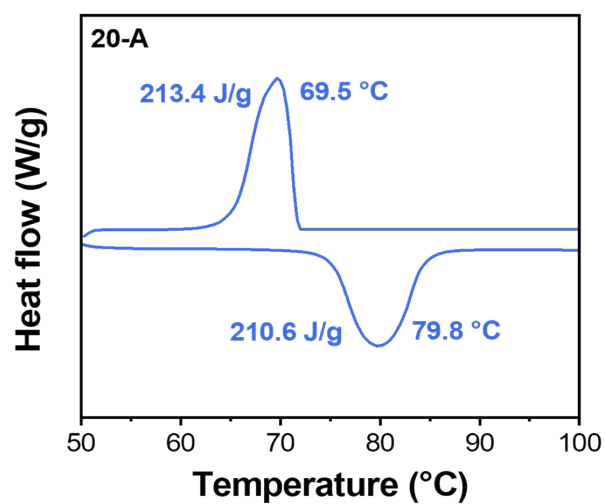


Fig. S18 DSC curve of 20-A

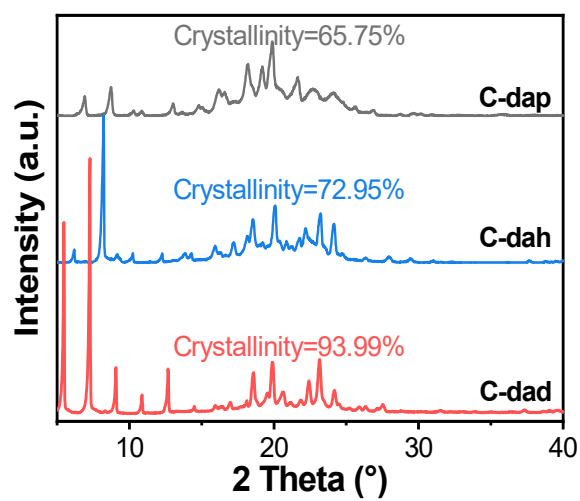


Fig. S19 XRD patterns of the benzoxazine-based PCMs

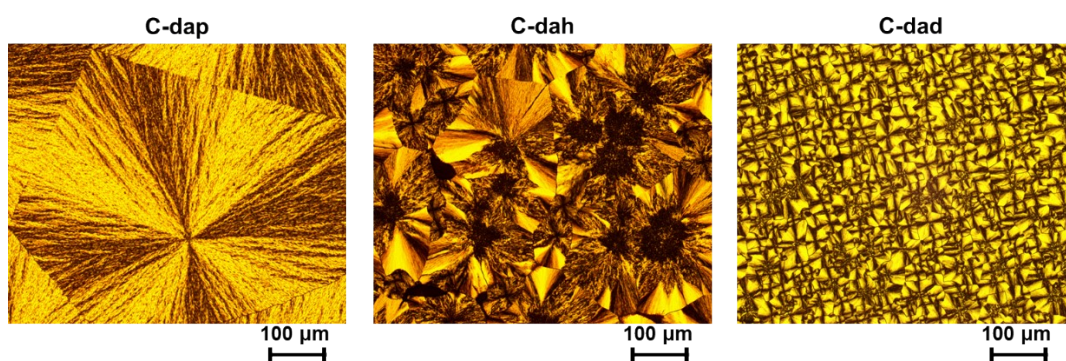


Fig. S20 POM images of different benzoxazine monomers

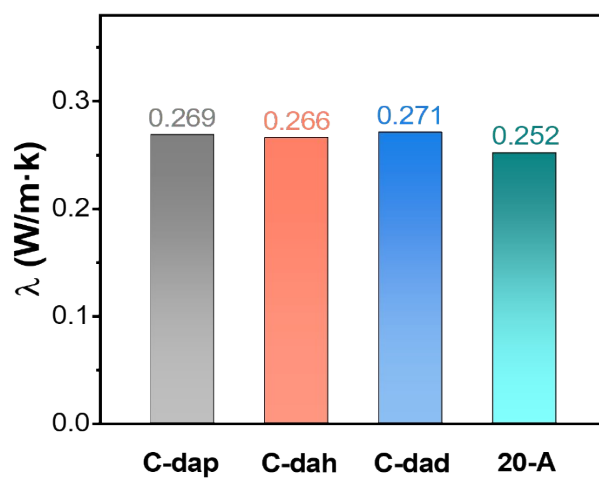


Fig. S21 Thermal conductivities (λ) of the benzoxazine-based PCMs and 20-A

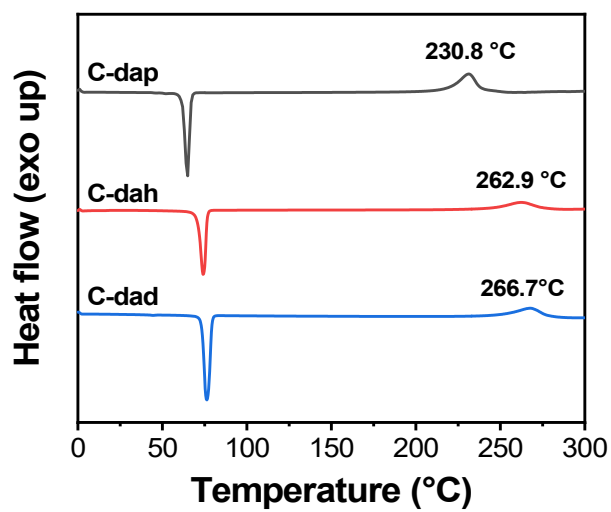


Fig. S22 ROP behaviors of different benzoxazine monomers based on DSC results

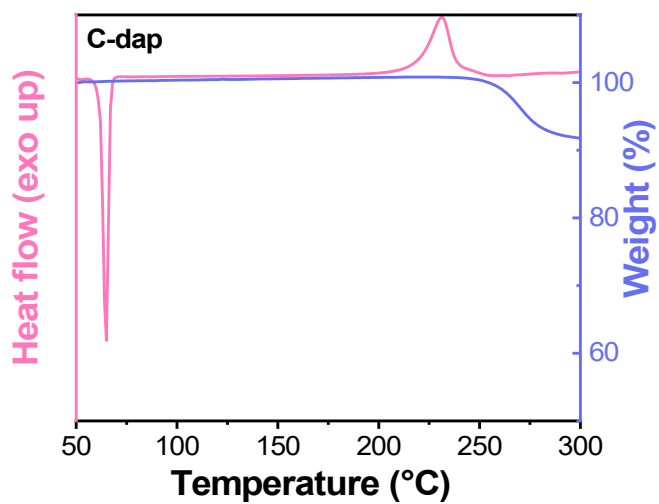


Fig. S23 DSC-TGA curves of C-dap

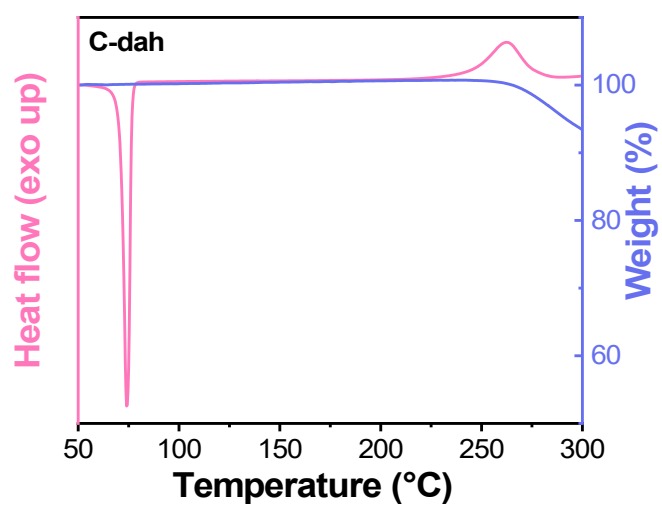


Fig. S24 DSC-TGA curves of C-dah

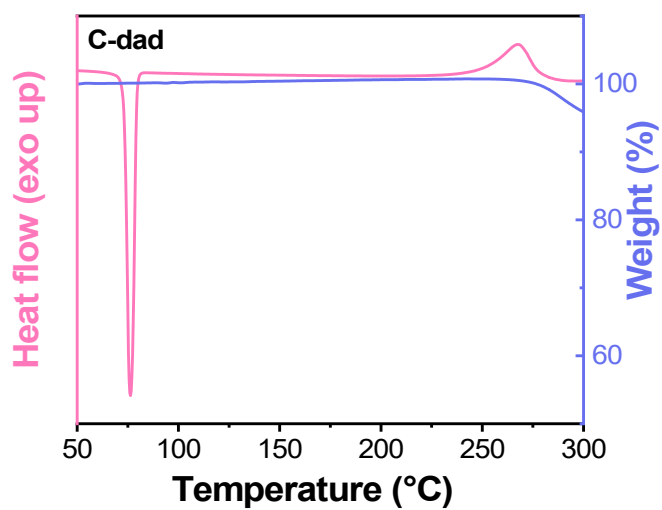


Fig. S25 DSC-TGA curves of C-dad

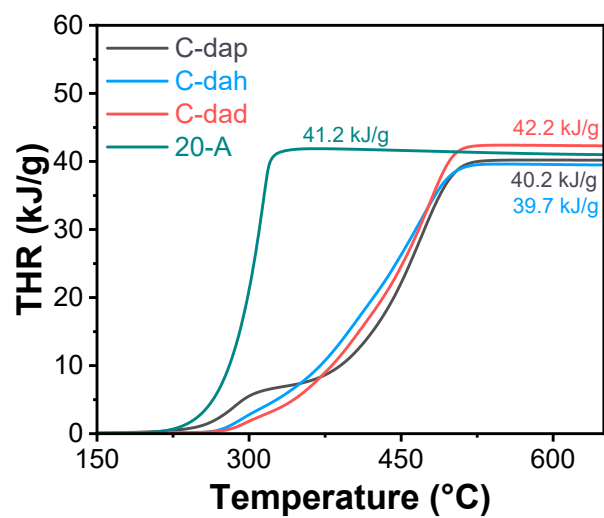


Fig. S26 THR curves of C-dap, C-dah, C-dad, and 20-A

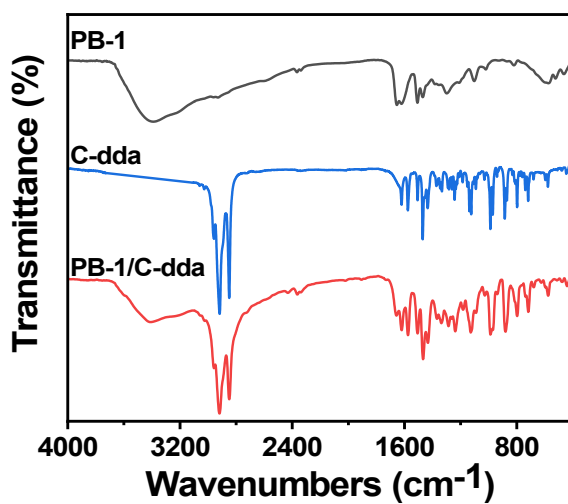


Fig. S27 FT-IR spectrums of PB-1, C-dad, and PB-1/C-dad

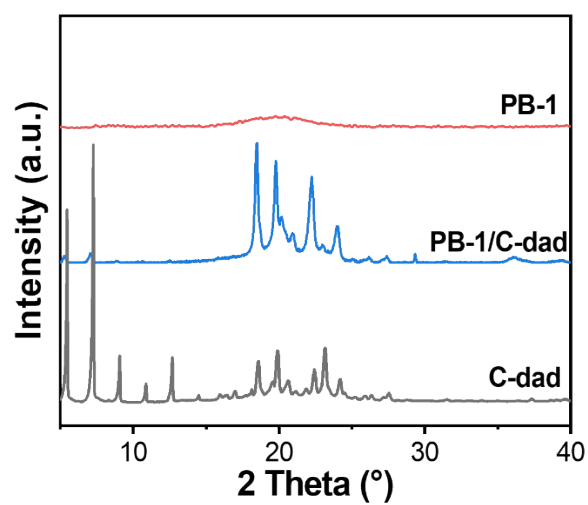


Fig. S28 XRD patterns of PB-1, C-dad, and PB-1/C-dad

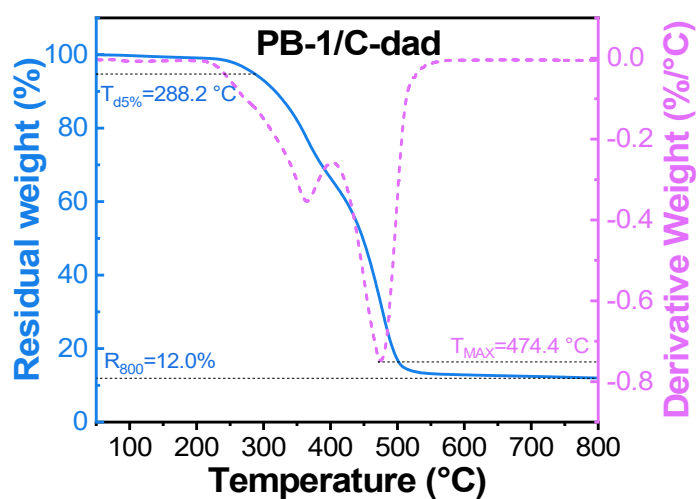


Fig. S29 TGA and DTG result of PB-1/C-dad

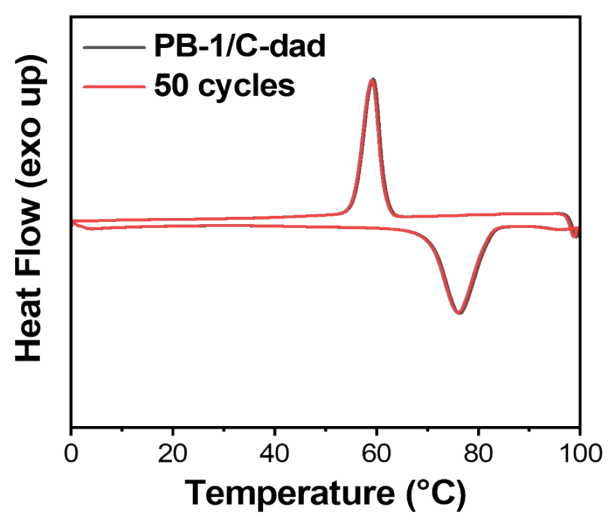


Fig. S30 Cycle stability of PB-1/C-dad

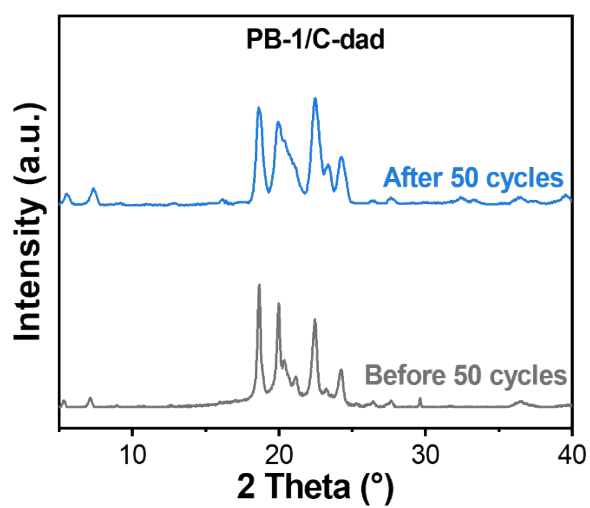


Fig. S31 XRD results of PB-1/C-dad before and after 50 thermal cycles

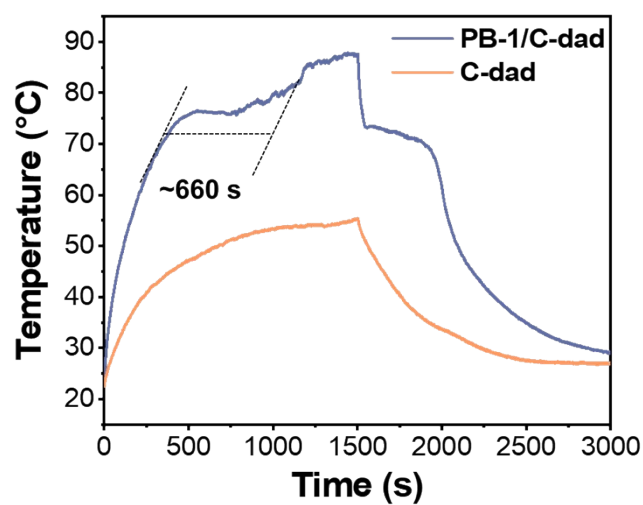


Fig. S32 Solar-to-thermal conversion curves of PB-1/C-dad and C-dad



Fig. S33 The char residues morphology of the PB-1/C-dad after igniting for 10 s

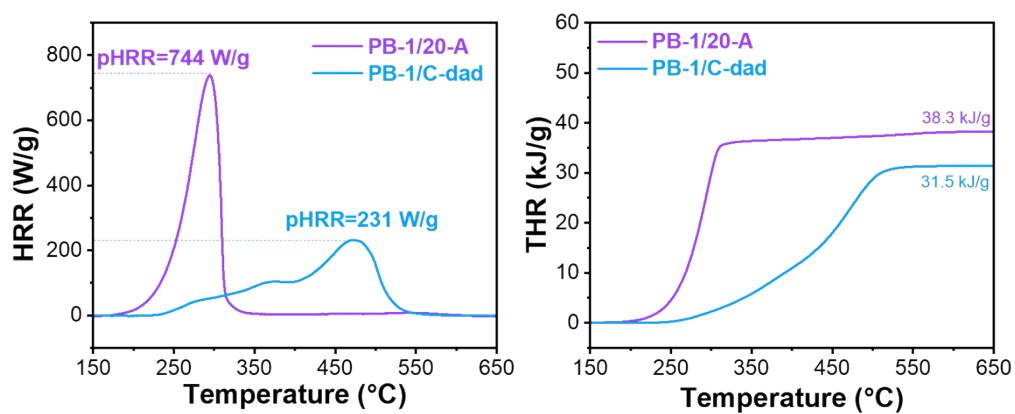


Fig. S34 MCC results of PB-1/20-A and PB-1/C-dad

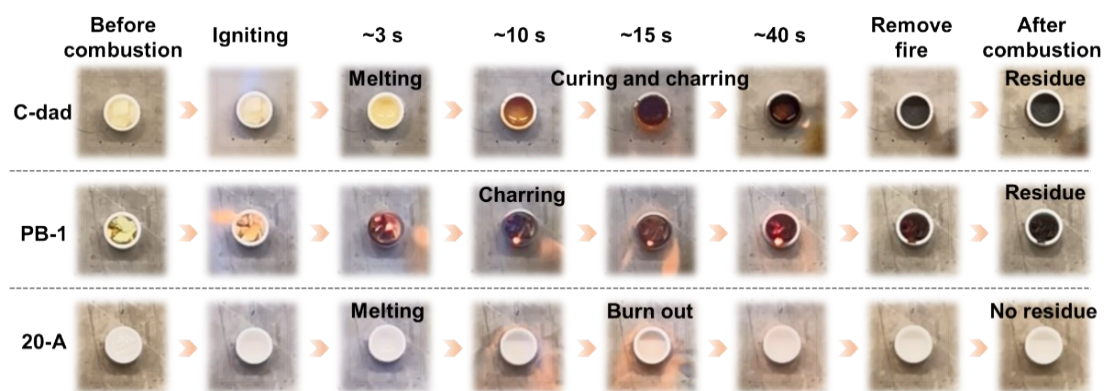


Fig. S35 Combustion tests of C-dad, PB-1, and 20-A

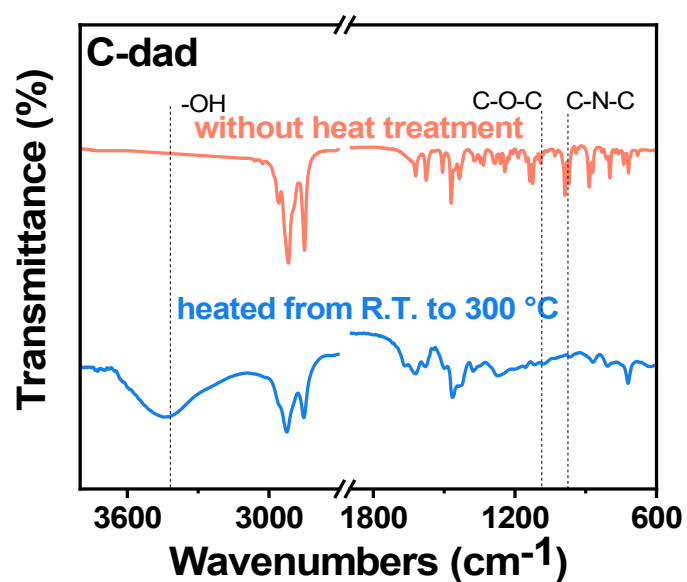


Fig. S36 FT-IR spectra of the pure C-dad and thermal-treated C-dad

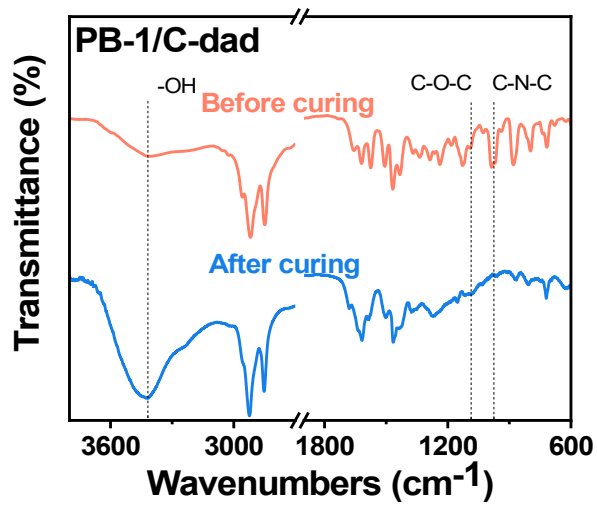


Fig. S37 FT-IR spectrums of PB-1/C-dad before and after curing

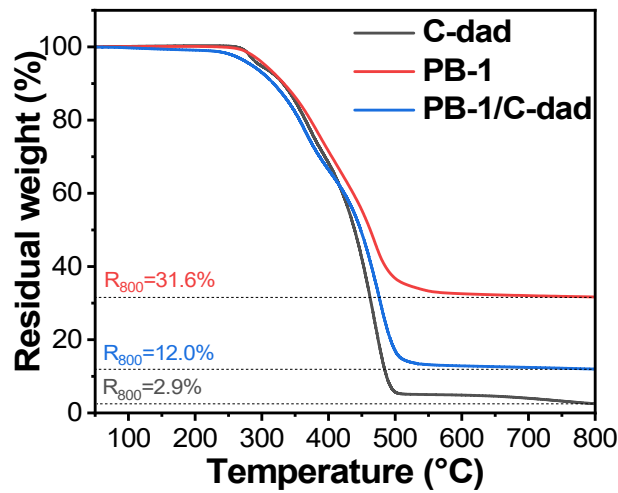


Fig. S38 TGA results of C-dad, PB-1, and PB-1/C-dad

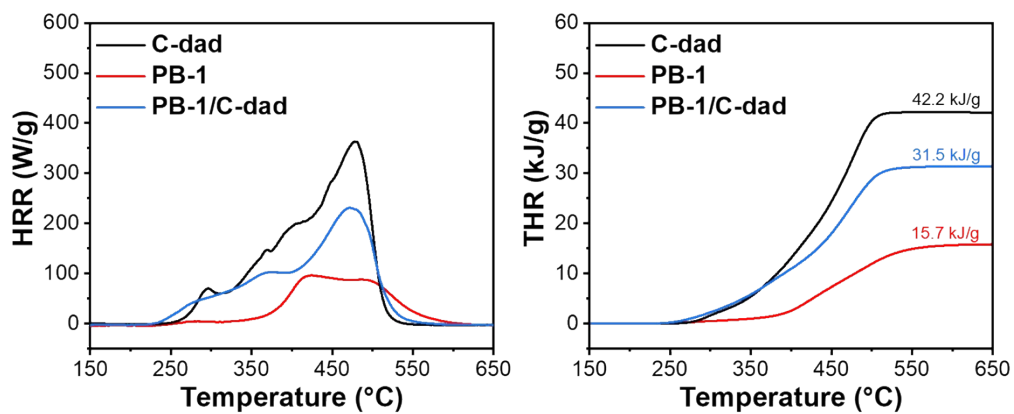


Fig. S39 MCC results of C-dad, PB-1, and PB-1/C-dad

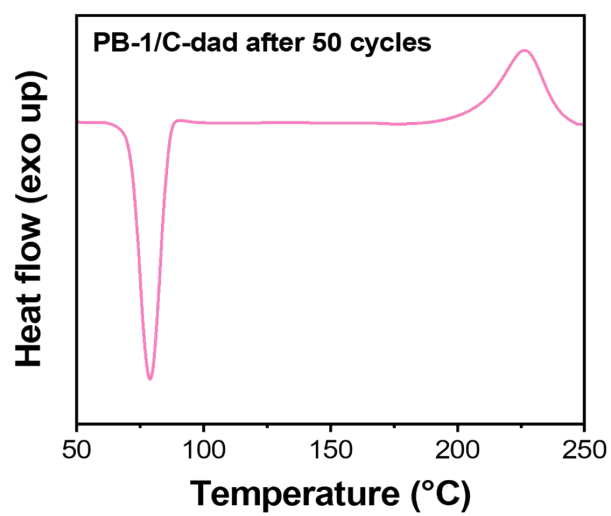


Fig. S40 DSC diagram of PB-1/C-dad after 50 cycles

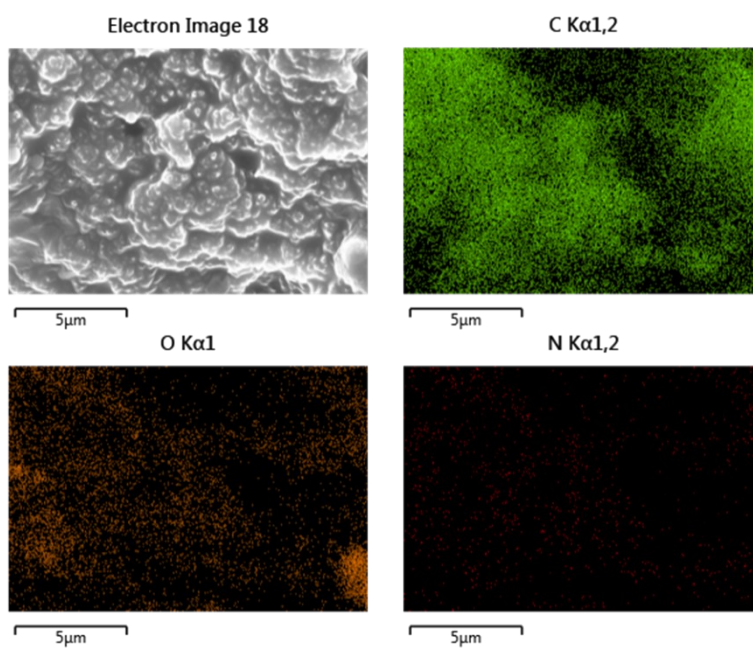


Fig. S41 Energy dispersive spectrometer of the char residues of PB-1/C-dad

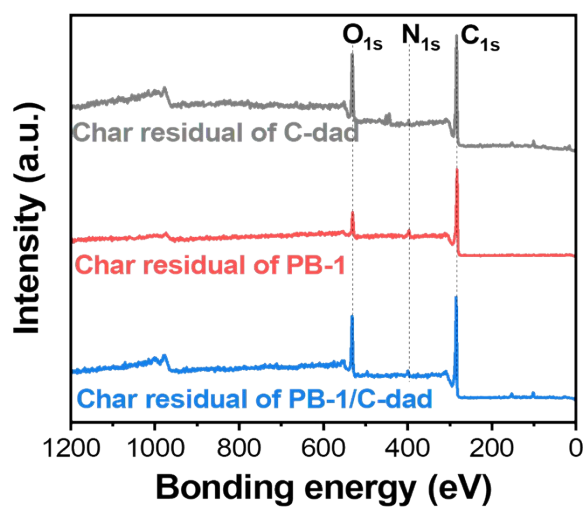


Fig. S42 XPS patterns of the char residues of C-dad, PB-1, and PB-1/C-dad

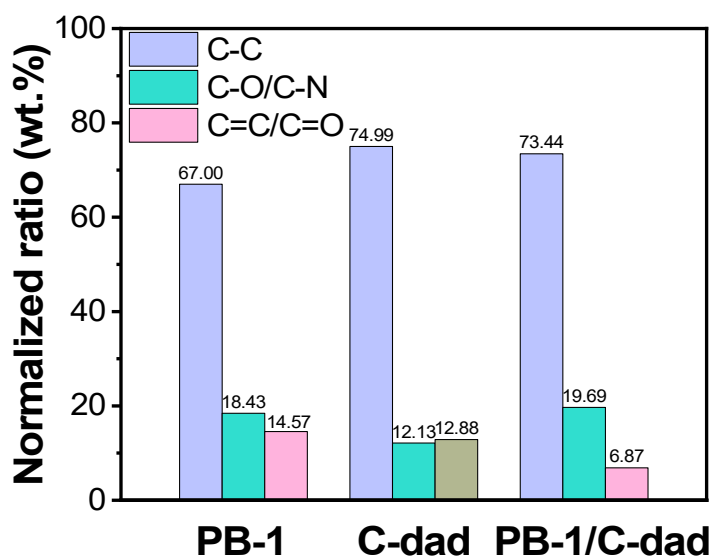


Fig. S43 Relative compositions of the chemical bonds in char residues of C-dad, PB-1, and PB-1/C-dad

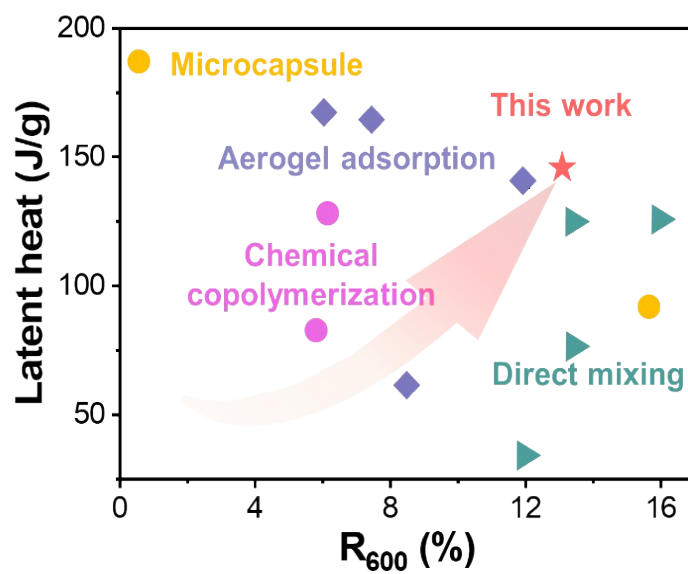


Fig. S44 Comparison of the R_{600} and latent heat of PB-1/C-dad with the representative polymer/organic PCM composites in the previous literature.

3. Equation S1-S5:

The loading rate was calculated by **Equation S1**:

$$R_l = \frac{m_{pcc} - m_{aerogel}}{m_{PCC}} \quad (S1)$$

where R_l is the loading rate of the PCMs, %; and m_{pcc} and $m_{aerogel}$ represent the mass of the phase change composite and aerogel, respectively, g.

The crystallization efficiency was calculated by **Equation S2**:

$$F_C = \frac{\Delta H_{PCMs}}{\Delta H_{PCC}} \quad (S2)$$

where F_C is the crystallization efficiency of the PCC, %; and ΔH_{PCMs} and ΔH_{PCC} represent the melting latent heats of the phase change materials and phase change composite, respectively, J/g.

The solar-to-thermal conversion efficiency was calculated by **Equation S3**:

$$\varphi = \frac{m \times \Delta H_m}{\rho_s \times S \times \Delta t} \times 100\% \quad (S3)$$

where m is the mass of the phase change composite, g; ΔH_m is the melting enthalpy of phase change composite, J/g; ρ_s is the power intensity of simulated solar (200 mW/cm²); S is the irradiation area of phase change composite, cm²; Δt is the time of the melting process.

The theoretical value of R_{800} of phase change material was calculated by **Equation S4**:

$$tR_{800} = mR_{800}^{PCMs} \times F_{PCMs} - mR_{800}^{aerogel} \times F_{aerogel} \quad (S4)$$

where tR_{800} is the theoretical R_{800} value of the PCC, %; mR_{800}^{PCMs} and $mR_{800}^{aerogel}$ represent the measured R_{800} values of the phase change materials and the aerogel, respectively, %; and F_{PCMs} and $F_{aerogel}$ stand for the mass fractions of the phase change materials and the aerogel, %.

The theoretical value of $pHRR$ of phase change material was calculated by **Equation S5**:

$$tpHRR = mpHRR_{PCMs} \times F_{PCMs} - mpHRR_{aerogel} \times F_{aerogel} \quad (S5)$$

where $tpHRR$ is the theoretical $pHRR$ value of the PCC, kJ/g; $mpHRR_{PCMs}$ and $mpHRR_{aerogel}$ represent the measured $pHRR$ values of the phase change materials and the aerogel, respectively, kJ/g; and F_{PCMs} and $F_{aerogel}$ stand for the mass fractions of the phase change materials and the aerogel, %.

4. Table S1-S4

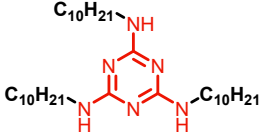
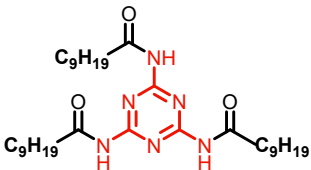
Table S1: Physical parameters of different aerogels

Samples	Mass concentrations of the precursor solutions (wt.%)	Density (g/cm ³)	Loading rate (%)	S _{BET} (m ² /g)	V _t (cm ³ /g)	V _m (cm ³ /g)
PB-1	2.8	0.140	83.6	107.4	0.50	0.27
PB-2	3.9	0.192	79.2	75.2	0.31	0.15
PB-3	4.8	0.256	75.3	60.3	0.22	0.11
PB-4	7.1	0.323	65.4	35.4	0.11	0.06

Table S2: Phase change performances of C-dap, C-dah, and C-dad

Samples	T _m (°C)	ΔH _m (J/g)	Melting range (°C)	T _c (°C)	ΔH _c (J/g)	Supercooling degree (°C)
C-dap	64.9	121.4	~11.4	33.2	119.5	31.7
C-dah	76.6	149.6	~12.5	54.9	145.5	21.7
C-dad	77.1	183.8	~10.8	60.7	171.7	16.4

Table S3: Comparison of the phase change performance and thermal stability of the benzoxazine-based PCMs with the synthetic PCMs containing phosphorus or nitrogen heterocycles in the previous literature.

Num.	Molecular structure	Melting point (°C)	Latent heat (J/g)	T _{d5%} (°C)	R ₆₀₀ (%)	Ref.
1		73.5	150.9	252	0	1
2		187.8	91.0	294	~10	

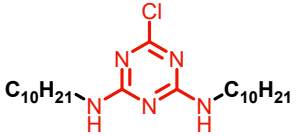
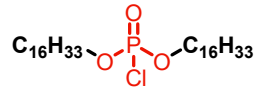
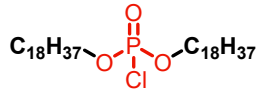
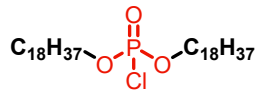
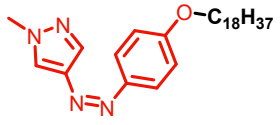
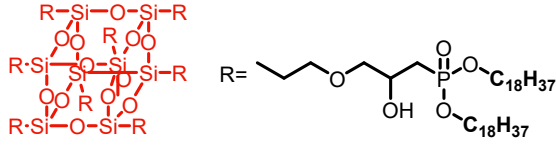
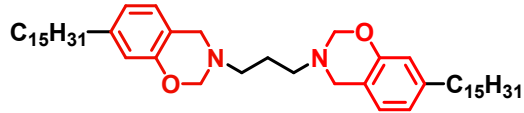
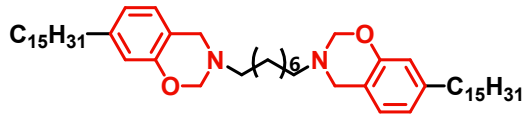
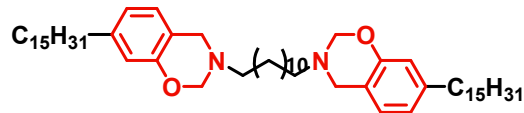
3		168.7	120.5	275	~6	
4		69	186.9	253	~10	2
5		73.5	156.4	236	~10	3
6		80	191.3	243.6	~9.5	4
7		74.0	171.7	~258	~0	5
8		52.88	116.9	175	16.3	6
9		64.9	121.4	271.6	14.7	
10		76.6	149.6	291.9	8.1	This work
11		77.1	183.8	302.8	4.8	

Table S4: Comparison of the phase change performance and thermal stability of the benzoxazine-based PCMs with the synthetic PCMs containing phosphorus or nitrogen heterocycles in the previous literature.

Num.	Main Polymer matrix	Main flame-retardant components	PCMs	PCC types	Latent heat (J/g)	pHRR (W/g)	R ₆₀₀ (%)	Ref.
1	Polyurethane	Cyclotriphosphazene group	PEG6000	Chemical copolymerization	81.5	362.8	5.75	7
2	Polyurethane	Black phosphorus nanosheets	PEG6000	Chemical copolymerization	127.3	442.3	6.14	8
3	Poly(urea-formaldehyde)	Phosphate group	Octadecane	Microcapsule	186.8	556.9	~0.5	9

4	polymethyl methacrylate	Carboxylated carbon nanotubes	Capric acid	Microcapsule	90.3	465.8	15.7	10
5	Acrylate polymer	DOPO group	PEG1000	Direct mixing	76.19	674	13.5	11
6	Polysiloxane	Phosphorus oxychloride	PEG2000	Direct mixing	124.7	~380	13.5	12
7	Polysiloxane	Phosphamide group	Paraffin	Direct mixing	125.2	539	16.0	13
8	Epoxy acrylate polymer	Dimethyl methyl phosphonate	Paraffin	Direct mixing	33.5	~225	~12	14
9	polyimide	Lignin-modified boron nitride	PEG4000	Aerogel adsorption	139.48	569.1	~12	15
11	Poly (vinyl alcohol)	Boron nitride/ ammonium polyphosphate	PEG2000	Aerogel adsorption	163.9	459.5	7.4	16
12	Phosphorylated poly (vinyl alcohol)	Phosphorylated group/graphene	PEG6000	Aerogel adsorption	60.9	557.5	8.5	17
14	Poly (vinyl alcohol)	Graphene	PEG2000	Aerogel adsorption	167.1	508.8	6.02	18
15	Polybenzoxazine	-	Benzoxazine monomer	Aerogel adsorption	145.3	230.5	13.1	This work

5. References

1. Z. M. Png, X. Y. D. Soo, M. H. Chua, P. J. Ong, J. Xu and Q. Zhu, *Journal of Materials Chemistry A*, 2022, **10**, 3633-3641.
2. R. Chen, X. Huang, R. Zheng, D. Xie, Y. Mei and R. Zou, *Chem. Eng. J.*, 2020, **380**, 122500.
3. Y. Luo, Y. Xie, H. Jiang, Y. Chen, L. Zhang, X. Sheng, D. Xie, H. Wu and Y. Mei, *Chem. Eng. J.*, 2021, **420**, 130466.
4. J. Li, R. Chen, Y. Luo, J. Shi, X. Sheng, Y. Xie, H. Wu, D. Xie and Y. Mei, *ACS Applied Energy Materials*, 2022, **5**, 1869-1882.
5. S. Wu, Z.-Y. Zhang, T. Li, R. Wang and T. Li, *ACS Materials Letters*, 2023, **5**, 2019-2027.
6. Y. Jiang, P. Yan, Y. Wang, C. Zhou and J. Lei, *Materials & Design*, 2018, **160**, 763-771.
7. X. Du, L. Jin, S. Deng, M. Zhou, Z. Du, X. Cheng and H. Wang, *ACS Applied Materials & Interfaces*, 2021, **13**, 42991-43001.
8. X. Du, J. Qiu, S. Deng, Z. Du, X. Cheng and H. Wang, *Renewable Energy*, 2021, **164**, 1-10.
9. Z.-T. Hu, V. H. Reinack, J. An, Z. Indraneel, A. Dasari, J. Yang and E.-H. Yang, *Langmuir*, 2021, **37**, 6380-6387.
10. S. Niu, M. Kang, Y. Liu, W. Lin, C. Liang, Y. Zhao and J. Cheng, *Energy*, 2023, **268**.
11. J. Liu, Y. Wuliu, X. Zhu, L. Zhang, J. Dai and X. Liu, *Compos. Sci. Technol.*, 2023, **238**, 110028.
12. Y. Qian, P. Wei, P. Jiang, Z. Li, Y. Yan and J. Liu, *Applied energy*, 2013, **106**, 321-327.
13. Y. Qian, P. Wei, P. Jiang and J. Liu, *Sol. Energy Mater. Sol. Cells*, 2012, **107**, 13-19.
14. P. Zhang, L. Song, K. Dai, X. Shan, H. Lu, J. Wang and Y. Hu, *Industrial engineering chemistry research*, 2011, **50**, 785-790.
15. R. Shen, L. Liu, Y. Cao, L. Zhang, X. Sheng and Y. Chen, *Solar Energy*, 2022, **242**, 287-297.
16. M. Zhou, D. Xie, K. Zhou, K. Gong, L. Yin, X. Qian and C. Shi, *Sol. Energy Mater. Sol. Cells*, 2022, **236**, 111537.
17. J. Shen, P. Zhang, L. Song, J. Li, B. Ji, J. Li and L. Chen, *Composites Part B: Engineering*, 2019, **179**, 107545.
18. L. Yin, D. Xie, K. Gong, C. Shi, X. Qian and K. Zhou, *ACS Applied Nano Materials*, 2023, **6**, 8752-8762.